haematologica
Journal of The Ferrata Storti Foundation

Daratumumab displays *in vitro* and *in vivo* anti-tumor activity in models of B cell non-Hodgkin lymphoma and improves responses to standard chemo-immunotherapy regimens

by Anna Vidal-Crespo, Alba Matas-Céspedes, Vanina Rodriguez, Cédric Rossi, Juan G. Valero, Neus Serrat, Alejandra Sanjuan Pla, Pablo Menéndez, Gaël Roué, Armando López-Guillermo, Eva Giné, Elías Campo, Dolors Colomer, Christine Bezombes, Jeroen Lammerts van Bueren, Christopher Chiu, Parul Doshi, and Patricia Pérez-Galán

Haematologica 2019 [Epub ahead of print]

Citation: Anna Vidal-Crespo, Alba Matas-Céspedes, Vanina Rodriguez, Cédric Rossi, Juan G. Valero, Neus Serrat, Alejandra Sanjuan Pla, Pablo Menéndez, Gaël Roué, Armando López-Guillermo, Eva Giné, Elías Campo, Dolors Colomer, Christine Bezombes, Jeroen Lammerts van Bueren, Christopher Chiu, Parul Doshi, and Patricia Pérez-Galán. Daratumumab displays in vitro and in vivo anti-tumor activity in models of B cell non-Hodgkin lymphoma and improves responses to standard chemo-immunotherapy regimens.
Haematologica. 2019; 104:xxx
doi:10.3324/haematol.2018.211904

Daratumumab displays *in vitro* and *in vivo* anti-tumor activity in models of B cell non-Hodgkin lymphoma and improves responses to standard chemo-immunotherapy regimens

Anna Vidal-Crespo[1*,a], Alba Matas-Céspedes[1,2*,b], Vanina Rodriguez[1], Cédric Rossi[3], Juan G. Valero[1,2], Neus Serrat[1,2], Alejandra Sanjuan-Pla[4], Pablo Menéndez[2,4,5], Gaël Roué[6], Armando López-Guillermo[2,7], Eva Giné[2,7], Elías Campo[2,8,9], Dolors Colomer[2,8], Christine Bezombes[10], Jeroen Lammerts van Bueren[11,c], Christopher Chiu[12], Parul Doshi[12,d] and Patricia Pérez-Galán[1,2]

[1] Department of Hematology-Oncology, Institut d'Investigacions Biomèdiques August Pi i Sunyer (IDIBAPS), Barcelona, Spain.
[2] Centro de Investigación Biomédica en Red-Oncología (CIBERONC), Barcelona, Spain.
[3] Department of Hematology, Dijon University Hospital, Dijon, France.
[4] Josep Carreras Leukemia Research Institute, Department of Biomedicine, School of Medicine, University of Barcelona, Barcelona, Spain.
[5] Institució Catalana de Recerca i Estudis Avançats (ICREA), Barcelona, Spain.
[6] Laboratory of Experimental Hematology, Department of Hematology, Vall d'Hebron Institute of Oncology, Vall d'Hebron University Hospital, Barcelona, Spain.
[7] Department of Hematology, Hospital Clínic-IDIBAPS, Barcelona, Spain.
[8] Hematopathology Unit, Department of Pathology, Hospital Clínic-IDIBAPS, Barcelona, Spain.
[9] Faculty of Medicine, University of Barcelona, Barcelona Spain.
[10] Centre de Recherches en Cancérologie de Toulouse (CRCT), UMR1037 INSERM, Université Toulouse III: Paul-Sabatier, ERL5294 CNRS, Université de Toulouse, Toulouse, France.
[11] Genmab, Utrecht, The Netherlands
[12] Janssen R&D, Spring House, PA.

*AV-C and AM-C contributed equally to this work.
[a] Current affiliation: MedImmune, Cambridge, UK
[b] Current affiliation: Grifols, Barcelona, Spain
[c] Current affiliation: Merus, Utrecht, The Netherlands
[d] Current affiliation: Bristol Myers Squibb, Lawrenceville, NJ

Running title: Daratumumab in B-NHL
Keywords: MCL, FL, DLBCL, CD38, Daratumumab, R-CHOP
Corresponding author: Patricia Pérez-Galán, PhD. Department of Hemato-Oncology, IDIBAPS. Rosselló 149-153, 08036. Barcelona, Spain. Email: pperez@clinic.cat

Counts:
Abstract: 250 words
Text: 3998
References: 48
Tables: 1 table
Figures: 6 main figures, 6 supplemental figures

ABSTRACT

CD38 is expressed in several types of non-Hodgkin lymphoma and constitutes a promising target for antibody-based therapy. Daratumumab (Darzalex) is a first-in-class anti-CD38 antibody approved for the treatment of relapsed/refractory multiple myeloma. It has also demonstrated clinical activity in Waldenström macroglobulinaemia and amyloidosis. Here, we have evaluated the activity and mechanism of action of daratumumab in preclinical *in vitro* and *in vivo* models of mantle cell lymphoma, follicular lymphoma and diffuse large B cell lymphoma, as monotherapy or in combination with standard chemo-immunotherapy. *In vitro,* daratumumab engages Fc-mediated cytotoxicity by antibody-dependent cell cytotoxicity and antibody-dependent cell phagocytosis in all lymphoma subtypes. In the presence of human serum, complement-dependent cell cytotoxicity was marginally engaged. We demonstrated by Selective Plane Illumination Microscopy that daratumumab fully penetrated a 3D lymphoma organoid and decreased organoid volume. *In vivo,* daratumumab completely prevents tumor outgrowth in models of mantle cell and follicular lymphoma, and shows comparable activity to rituximab in a disseminated *in vivo* model of blastic mantle cell lymphoma. Moreover, daratumumab improves overall survival in a mouse model of transformed $CD20^{dim}$ follicular lymphoma, where rituximab showed limited activity. Daratumumab potentiates the antitumor activity of CHOP and R-CHOP in mantle cell and follicular lymphoma xenografts. Furthermore, in a patient-derived diffuse large B cell lymphoma xenograft model, daratumumab anti-tumor activity was comparable to R-CHOP and the addition of daratumumab to either CHOP or R-CHOP led to full tumor regression. In summary, daratumumab constitutes a novel therapeutic opportunity in certain scenarios and these results warrant further clinical development.

ARTICLE SUMMARY

- Pre-emptive daratumumab completely prevents tumor outgrowth in xenograft models of MCL and FL
- Therapeutic daratumumab improves overall survival in a mouse model of transformed $CD20^{dim}$ FL greater than rituximab, and potentiates the antitumor activity of CHOP and R-CHOP in MCL and FL xenografts; in a patient-derived DLBCL xenograft model, daratumumab activity was comparable to R-CHOP and the addition of daratumumab to either CHOP or R-CHOP led to full tumor regression.

INTRODUCTION

B cell non-Hodgkin's lymphoma (NHL) constitutes 4-5% of all hematologic neoplasia with increasing incidence in western countries.[1] Diffuse large B-cell lymphoma (DLBCL) and follicular lymphoma (FL) represent the most frequent aggressive and indolent NHL, accounting for approximately 35% and 20 % of all lymphomas, respectively.[2,3] Moreover, roughly one third of FL patients develops histologic transformation (tFL) to DLBCL leading to a dismal prognosis.[4] Both entities are currently treated with chemo-immunotherapy including a rituximab backbone.[5,6] FL responses are usually high, although recurrence occurs in the majority of the cases.[7] In DLBCL, currently classified into germinal center type (GCB) or activated B-cell type (ABC),[8] treatment is not guided by subtype, and responses to chemo-immunotherapy are normally higher in the GCB subtype. Nevertheless, a portion of DLBCL (20%) do not respond to this regimen.[9] Several second-generation anti-CD20 antibodies, such as the FDA-approved obinutuzumab have been clinically tested to overcome these limitations.[10,11] However, an alternative evolving therapeutic approach is to target a different antigen. In this regard, both FL and DLBCL originate in the germinal center (GC) and consequently express high levels of CD38, making this molecule an attractive therapeutic target.[12]

Mantle cell lymphoma (MCL) is a rare NHL (6% of all NHL) with an aggressive evolution and clinically challenging.[13,14] Its frontline therapy, although heterogeneous, typically consists of rituximab-based chemo-immunotherapy followed by autologous-stem cell transplantation and/or rituximab maintenance. Even with intensive therapy, MCL patients ultimately relapse.[15] Novel targeted therapies currently approved for relapsed/refractory (R/R) MCL include[14] the mTOR inhibitor temsirolimus, the immunomodulatory agent lenalidomide, the proteasome inhibitor bortezomib,[16] also approved in front-line, and the BTK inhibitor ibrutinib that achieves the highest response rates.[17] However, MCL patients failing ibrutinib treatment have very limited therapeutic options.[18] In this situation, where virtually all MCL cases express some level of CD38, this antigen represents a potential alternative target to be explored. Moreover, CD38 is associated with nodal disease and poorer survival [19,20] and high CD38 expression correlates with poor *in vivo* response to bortezomib[21]. Thus, targeting CD38 could hold promise as a strategy for MCL, also in bortezomib resistant tumors.

CD38 is present at high levels in bone marrow (BM) precursor cells and it is downregulated in resting normal B cells. The molecule is re-expressed at high density once naïve B-lymphocytes are activated, and peaks when B cells enter the GC. Terminally differentiated plasma cells and their pathological counterparts express the highest surface density among human cells, while it is completely absent in memory B cells.[22] CD38 behaves simultaneously as an enzyme and as

a receptor. The extracellular domain of CD38 contains an enzymatic site that can generate cyclic ADP ribose (cADPR) and ADPR from nicotine adenine dinucleotide (NAD+). This control of adenosine synthesis by CD38 may be important in the context of the characteristic immunosuppressive tumor microenvironment.

Daratumumab (Darzalex) is a first-in-class, human IgG1κ monoclonal antibody that targets the CD38 epitope. It was approved by the U.S. FDA in 2015 as a monotherapy for patients with multiple myeloma (MM), who have received at least 3 prior therapies.[23] Currently, daratumumab has been approved in combination with dexamethasone plus either lenalidomide or bortezomib, or pomalidomide for the treatment of relapsed MM patients.[24] Daratumumab has a broad-spectrum killing activity in MM engaging complement-dependent cytotoxicity (CDC), antibody-dependent cellular cytotoxicity (ADCC),[25] antibody-dependent cellular phagocytosis (ADCP),[26] and apoptosis.[27] Moreover, daratumumab modulates the enzymatic activity of CD38[28] and induces an immunomodulatory role in MM by depleting $CD38^+$ immune suppressive cells[29] contributing to its antitumor activity. In chronic lymphocytic leukemia (CLL), we have demonstrated that daratumumab induces cytotoxic activity *in vitro via* ADCC and ADCP in primary CLL cells and cell lines. *In vivo*, Daratumumab significantly prolongs overall survival of animals in systemic CLL murine models. Daratumumab also affects tumor-microenvironment interactions by blocking CLL homing and dissemination to secondary lymphoid organs *in vitro* and *in vivo*.[30]

In the present study, we aimed to investigate *in vitro* and *in vivo* activity of daratumumab on MCL, FL and DLBCL cells as monotherapy and in combination with standard therapies.

METHODS

Therapeutic drugs

Daratumumab (Darzalex, anti-CD38mAb, IgG1) and the isotype control mAb (CNTO 3930, IgG1) were provided by Janssen. Rituximab (Mabthera, anti-CD20 mAb, IgG1) and the chemotherapy regimen CHOP (cyclophosphamide, doxorubicin, vincristine, and prednisone) were obtained from the department of pharmacy of the Hospital Clínic of Barcelona.

Subcutaneous pre-emptive mouse models

SCID mice (Janvier Laboratories) were subcutaneously (sc) injected with $10x10^6$ RL-luc cells in the FL model or $10x10^6$ REC-1 cells in the MCL model, respectively, following a protocol approved by the Animal Testing Ethic committee of the University of Barcelona and Generalitat de Catalunya (Protocol # 9971). Mice were randomly assigned into cohorts of 6 mice per group and received one intraperitoneal (ip) injection of 10 mg/kg of daratumumab or isotype control every other week, starting the day of cell inoculation.

Patient-derived DLBCL xenograft model

ST1361 is a DLBCL patient-derived xenograft model developed using a DLBCL tumor originated in a metastatic site from a 58-year-old chemotherapy-naïve Hispanic male. ST1361 was GCB subtype transformed from an Epstein-Barr virus negative FL tumor.

The DLBCL tumor was homogeneously chopped into fragments of similar size and injected sc into SCID mice. Treatment was initiated when mean tumor volume was approximately 150-250 mm^3. Daratumumab 20 mg/kg was administered weekly for 3 weeks alone or in combination with CHOP (20 mg/kg cyclophosphamide, 1.25 mg/kg doxorubicin, 0.2 mg/kg vincristine [intravenously on Day 0], and 0.15 mg/kg prednisone [Days 0-4]; QD for 5 days) or R-CHOP (10 mg/kg rituximab [intraperitoneally on Day 0]+ CHOP as before).

Statistical analysis

Unpaired and paired *t*-tests were used to assess statistical differences between two groups using GraphPad Prism software 4.0. For Kaplan-Meier survival curves, SPSS19 software was used. Additional methodologic details are described in Supplementary Methods.

Additional material and methods are available as supplementary information

RESULTS

Daratumumab induces cell killing in the presence of external effectors in B-NHL

We first assessed by calcein-AM release assay, the ability of daratumumab to induce ADCC, ADCP and CDC in MCL, FL and DLBCL cell lines. Using peripheral blood mononuclear cells (PBMCs) from healthy donors as external effectors we demonstrated that daratumumab engages ADCC in a panel of B-NHL cell lines (Table 1). Daratumumab induced a significant dose-dependent cell lysis reaching its maximum antitumor activity at 1 µg/mL on MCL cell lines (mean ± SD = 45% ± 14%) (Fig. 1A), at 0.1 µg/mL on FL cell lines (mean ± SD = 48% ± 18%) (Fig. 1B), and at 0.1µg/mL on DLBCL cell lines (mean ± SD = 49% ± 11%) (Fig. 1C). The degree of ADCC induction did not correlate with the number of CD38 molecules per NHL cell (sABC) (specific Antibody Binding Capacity) (r^2 = 0.1988; Fig. S1A and Table 1). A phagocytosis assay using mouse macrophages as effector cells was set up to determine daratumumab-mediated ADCP. Daratumumab induced significant ADCP at 1 µg/mL in MCL cell lines (mean ± SD = 54% ± 24; Fig. 1D) FL cell lines (mean ± SD = 64% ± 26; Fig. 1E), and in DLBCL cell lines (mean ± SD = 39% ± 18; Fig. 1F). The degree of ADCP induction neither correlated with the number of CD38 sABC on NHL cell lines (r^2 = 0.2270; Fig. S1B and Table 1).

Interestingly, the daratumumab-opsonized cells that were exposed to macrophages and not phagocytosed, suffered a lost in CD38 surface expression, irrespective of the degree of ADCP induction (Figure S2), in a process that may resemble trogocytosis as previously described in MM studies.[31,32]

We next evaluated the CDC activity and observed that, similar to that reported for CLL cells,[30] daratumumab induced low to marginal cell death in the presence of normal human serum (NHS 10%) (Table 1). Very similar results were obtained in these CDC experiments when 50% NHS was applied. The high expression of the complement regulatory proteins (CRPs) CD46, CD55 and CD59, and an insufficient number of CD38 molecules per cell on NHL cells may explain the low CDC activity (Table 1).

Collectively, daratumumab effectively kills $CD38^+$ NHL cells through engagement of ADCC and ADCP but not CDC, independently of the expression levels of CD38.

Daratumumab enters and distributes homogeneously within a 3D lymphoma model

To model the compact aggregates of lymphoma cells growing in the patients' lymph nodes, 3D spheroids were generated by the hanging drop method,[33] using RL-GFP cells previously reported as an useful tool for antibody therapy studies.[34] We first sought to determine the degree to which daratumumab can penetrate these lymphoma aggregates depending on dose

(1 and 10 µg/mL mAb) and time of exposure (4, 24 and 48 hours). First, we measured the percentage of mAb diffusion in the spheroid, representing the total quantity of the mAb in the spheroid. Three-dimensional (3D) reconstruction images obtained by SPIM (Fig. 2A) revealed a maximum diffusion of daratumumab at 1 µg/mL after 48 hours of treatment (Fig. 2B). Next, maximum depth of daratumumab in the spheroids was determined under the same conditions and represented as percentage of mAb penetration in the spheroid. As observed for the diffusion, a maximum penetration of daratumumab at 1 µg/mL after 48 hours of treatment was achieved (Fig. 2C). Moreover, a significant dose-dependent reduction of the spheroid volume was observed after daratumumab treatment compared to isotype control (mean ± SD = 15% ± 6%, 20% ± 7%, respectively at 1 and 10 µg/mL) (Fig. 2D) showing a direct effect of daratumumab on tumor growth in 3D. This observation was validated in additional lymphoma cell lines. Daratumumab moderately but significantly ($p<0.0001$) reduced the spheroid volume in all the cell lines analyzed, albeit in a different degree (Fig S3A-B), that was accompanied in most of cases by a concomitant decrease in the cell number. However, this observation did not apply to HBL-2 and WSU-DLCL2 cell lines, where daratumumab may just generate a tighter spheroid (Fig S3C).

These data demonstrate that daratumumab efficiently penetrates a lymphoma 3D structure and moderately reduces the growth of spheroids in the absence of external effectors.

Daratumumab prevents tumor outgrowth in MCL and FL xenografts

As a first test of daratumumab activity *in vivo* in NHL models, we inoculated SCID mice sc with two cell lines that we have previously set up, RL cells to model transformed FL (tFL),[35] and REC-1 cells to model MCL.[36] SCID mice have active NK cells and macrophages that can act as effector cells to engage daratumumab activity, as we have shown using *in vitro* models. Mice were treated with daratumumab or isotype control (20 mg/kg) starting on the day of tumor injection. Subsequently, animals received antibody injections every other week (10 mg/kg) for a total of three doses and were sacrificed at day 30 (REC-1) (Fig. 3A) or day 34 (RL) (Fig. 3B). Daratumumab prevented tumor formation in all mice injected with REC-1, and in 5 out of 6 mice injected with RL cells. In this latter model, a $20mm^3$ RL tumor was found in one daratumumab-treated mouse at the endpoint (day 34). As the RL cells inoculated expressed the luciferase gene, bioluminescence analysis at different time points further supported these results (Fig. 3B). All animals receiving isotype control antibody formed tumors of at least $100mm^3$ within a mean of 18 days (REC-1) and 21 days (RL) and were bigger than 1000 mm^3 at the end of the experiment.

Daratumumab prolongs overall survival and reduces tumor infiltration in systemic xenograft models of MCL and FL

Next, we generated a model for blastic MCL by inoculating Z-138 cells intravenously into SCID mice, and one-week later mice were treated weekly with either daratumumab (D), rituximab (R) or isotype (I) control (20/10/10/10 mg/kg). Seven out of ten isotype-treated mice had to be sacrificed between days 57 - 89 due to systemic signs of disease (Fig. 4). Daratumumab significantly improved overall survival (OS) (I *vs* D: ***p< 0.001), with 90% of the mice treated with daratumumab surviving for over 107 days, (Fig. 4A) compared to just 10 % alive in the controls. OS for the daratumumab group was slightly superior but did not reach statistical significance (D *vs* R: ns p = 0.2907), compared to that observed in the rituximab-treated mice (I *vs* R: **p<0.01), where 70% of the mice were alive at day 107 (Fig. 4). Mean survival was 73 days for the control group, 97 for rituximab and 103 for daratumumab groups. On autopsy, the disease had spread to brain, BM, spleen and lungs (Fig. S4A). Daratumumab treatment reduced the disease burden in brain, BM, and spleen by 93%, 63%, and 48%, respectively (Fig S4B). Rituximab-treated mice showed a similar reduction in tumor load to that achieved by daratumumab in brain (73%) and BM (69%) compared to that observed with the isotype control, while no effect was observed in spleen infiltration. Finally, daratumumab did not diminish lung infiltration, while a moderate reduction was seen in rituximab-treated mice (18%) compared to isotype control mice (Fig. S4B), suggesting organ-dependent differential immunotherapeutic response.

In the FL systemic model, $CD20^{low}$ WSU-FSCCL cells (Table 1) were intravenously inoculated in SCID mice and one-week later mice were treated weekly with daratumumab, rituximab or isotype control (20/10/10/10 mg/kg). All control-treated and rituximab-treated mice rapidly succumbed to the disease and died or had to be euthanized due to severe disease signs by day 40 (control group) and day 62 (rituximab group), respectively (Fig. 4). In contrast, in the daratumumab-treated group, OS was significantly prolonged (I *vs* D: ***p< 0.001 I *vs* R: **p<0.01; D *vs* R *p< 0.05*)*. Mean survival was 35 days for the control group, 41 for rituximab and 60 for daratumumab. By the end of the experiment (day 90), 30% of mice treated with daratumumab were cured (Fig. 4). On autopsy, WSU-FSCCL cells showed systemic dissemination of disease in brain, BM and spleen (identified as $huCD45^{+}/CD19^{+}/CD10^{+}$; Fig. S4C). Daratumumab robustly decreased dissemination to brain (90%, p< 0.01) as compared to the control group, while rituximab was not effective (Fig. S4D). Homing of WSU-FSCCL cells to the spleen and BM was less prominent. There were no significant differences in the reduction

of dissemination to spleen and BM by daratumumab compared to the rituximab-treated group (Fig. S4D).

Altogether, these data confirm that daratumumab shows comparable to superior activity with respect to rituximab in systemic models of MCL and FL

Daratumumab synergizes with R-CHOP to reduce tumor burden in preclinical models of MCL and FL

The synergy between daratumumab and rituximab and/or chemotherapy regimens was evaluated in MCL (REC-1) and tFL (RL) xenograft heterotopic models. SCID mice were inoculated subcutaneously with NHL cells and when tumors became palpable, mice were randomly assigned into the following groups: i) Isotype ii) daratumumab iii) CHOP iv) D-CHOP v) R-CHOP and vi) R-D-CHOP. Tumor volume was assessed twice a week and tumor weights at sacrifice. In the MCL model (Fig. 5A), daratumumab induced significant anti-tumor activity compared to the isotype control (42%, $p< 0.01$). CHOP alone marginally reduce tumor growth ($p = 0.182$) and no difference was observed between daratumumab and D-CHOP groups ($p = 0.451$). Importantly, adding rituximab to D-CHOP treatment (R-D-CHOP) induced a significant reduction in tumor volume compared to the isotype control (86%, $p< 0.001$) and also compared to R-CHOP (73% $p < 0.001$) and D-CHOP (51%, $p < 0.05$) alone. Similarly, in the tFL model (Fig. 5C-D), daratumumab treatment inhibited tumor growth compared to isotype control (36%, $p< 0.001$). On the other hand, the combination D-CHOP inhibited tumor growth significantly better than daratumumab as a single agent (57%, $p< 0.001$), resembling that achieved by R-CHOP (67%, $p< 0.001$). In addition, the combination regimen of R-D-CHOP had a remarkable effect in impeding tumor growth (84% inhibition, $P< 0.001$), which was superior than that achieved by each combination regimen separately ($p< 0.001$). The results of the RL-luc model were further validated by bioluminescence and quantification of the signal captured at the endpoint (Fig. S5A-B). Moreover, tissue sections of selected mice of each group were analyzed by immunohistochemistry for the proliferation marker pH3 and the angiogenesis marker CD31, further confirming these results (Fig. S5C).

In conclusion, these data demonstrate the value of the combination R-D-CHOP as a new therapeutic strategy in MCL and tFL superior to the standard of care (R-CHOP)

Daratumumab induces tumor growth inhibition and prolongs survival in a patient-derived DLBCL xenograft model in combination with R-CHOP

To further evaluate the activity of daratumumab alone or in combination with the standard-of-care therapy we used a clinically more relevant patient-derived DLBCL xenograft model

(ST1361) with detectable CD38 expression by immunohistochemistry (Fig S6). Identical to the MCL and tFL models, all individual treatments were capable of reducing tumor volume over time ($p<0.001$, Fig 6A); however, daratumumab alone was strikingly efficient with an anti-tumor activity comparable to R-CHOP ($p<0.001$, Fig 6A). Furthermore, the addition of daratumumab to either CHOP or R-CHOP led to full tumor regression ($p<0.001$, Fig 6A). Importantly, tumor volume negatively correlated very well with the OS of xenograft-bearing mice, regardless the treatment group (Fig 6B). Thus, mice treated with either daratumumab alone or R-CHOP displayed identical OS and, in line with the full tumor regression achieved, daratumumab combined with either CHOP or R-CHOP resulted in 100% survival at the end of the experiment ($p<0.05$ after Bonferroni multiplicity correction, Fig 6A). Remarkably, full tumor regression and 100% a survival at day 60 were observed even when daratumumab treatment was ceased as early as 14 days (total of 3 doses) after tumor cell inoculation. Collectively, these results indicate that tumor cells were completely eliminated within a short time and that no tumor escape occurred in this DLBCL patient-derived model.

DISCUSSION

In this study we have demonstrated that daratumumab engages Fc-mediated cell killing of NHL cells by ADCC and ADCP. Variation in the extent of ADCC and ADCP could not be explained by the differences in CD38 expression levels. Similar observations were also reported for daratumumab-induced ADCC and ADCP in CLL cells.[30] The capacity of daratumumab to induce ADCC and phagocytosis may to some extent be related to other factors, such as the expression of different types of FcγR, KIRs and Natural Cytotoxic Receptors (NCR) on NK cells.[37] Moreover, the expression of the so-called 'don't eat me' signals, such as CD47, on tumor cells plays an important role in regulating phagocytosis. In fact, CD47 expression has been found to be increased on MCL, FL and DLBCL cells compared to normal cells, conferring a worse clinical prognosis.[38] Moreover, in agreement with previous results in MM, [32] the daratumumab-opsonized cells that were exposed to macrophages and not phagocytosed, suffered a lost in CD38 surface expression. This event may reduce the ability of daratumumab to kill lymphoma cells *via* CDC and ADCC, compromising the therapeutic efficacy of daratumumab. However, MM studies demonstrated that this phenomenon occurs early in the treatment irrespective of their clinical responses.[32] Therefore, CD38 reduction *via* trogocytosis should not necessarily be considered as an escape mechanism from daratumumab treatment. On the contrary, trogocytosis may be beneficial and represent a novel mechanism of action of daratumumab, as in this process there is also transfer of tumor cell membrane fragments containing important

signaling molecules such as CD56 CD49d and CD138. The decreased expression of these adhesion molecules in tumor cells may compromise their interaction with tumor microenvironment as we reported in a previous work. [30]

Daratumumab did not induce CDC in FL, or DLBCL or MCL cell lines. Flow cytometry analysis demonstrated that MCL and FL cells show medium to high expression of CD38 while DLBCL cells tend to express higher levels of CD38. However, the number of molecules per cell in these NHL cell lines was lower than that found on the CDC-sensitive Daudi Burkitt lymphoma cell line, suggesting a threshold for CD38-targeted CDC lysis. In addition, this low induction of CDC was also associated with high expression of the CRPs CD55 and CD59 that were lower in Daudi cells. These observations are in line with our previous data obtained for CLL cell lines and primary cells.[30] Overall, baseline expression of CD38/CD55/CD59 appears to be associated with response to daratumumab-induced CDC *in vitro in* FL, DLBCL and MCL cells. These results mirrored those obtain with the anti-CD20 rituximab in CLL cells.[39]

We have shown for the first time that daratumumab, at clinically achievable doses, effectively penetrates a lymphoma organoid *in vitro* model. A moderate but significant reduction of the sphere volume was observed with daratumumab in 3D models of lymphoma, even though no significant effect was observed in a 2D model (data not shown). These results agree with daratumumab efficacy against subcutaneous tumors *in vivo* (Figs 5 and 6).

In vivo results support the ability of daratumumab to prevent the outgrowth of MCL and FL cells, when administered in a prophylactic setting, prior to tumor development. These results open a window of opportunity for daratumumab as an alternative to rituximab maintenance therapy in these models, in the context of a complete response after the induction therapy.[40,41] Moreover, we have demonstrated that daratumumab shows single agent activity both in systemic and subcutaneous models of NHL, when administered after disease onset. More importantly, the data from the FL model using WSU-FSCCL cells point to a possible role for daratumumab as a therapeutic alternative to rituximab in NHLs with reduced CD20 expression. Previous studies have shown a substantial and rapid reduction of CD20 in lymphoma patients treated with rituximab, which has been linked to development of acquired resistance.[42,43] Thus, daratumumab treatment may be considered in these scenarios where anti-CD20 resistance has developed due to antigen shaving.[44] In addition, our results indicate that daratumumab significantly improves long-term survival when used as a single agent, indicating that it may be also an alternative to rituximab in NHL $CD20^{high}$, evidenced by the comparable activity of both antibodies in the blastic MCL model using Z-138 cells. We have also observed a remarkable effect of daratumumab in the tumor cell dissemination to brain in FL and MCL

systemic models. This may be related to the capacity of daratumumab to cross the hemato-encephalic barrier. In fact, daratumumab has shown efficacy in CNS plasmocytoma[45] and extramedullary myeloma.[46]

Finally, we have examined the combination of daratumumab with the standard of care therapy R-CHOP. Our data suggest that daratumumab significantly potentiates R-CHOP activity, inducing higher rates of tumor regression in MCL and FL. Moreover, we analyzed the efficacy of daratumumab in a DLBCL patient derived mouse xenograft, generated from a transformed FL, and usually less responsive to chemotherapy, as shown in our results where indeed the CHOP regimen displayed limited activity. In this model, daratumumab in combination just with CHOP, in the absence of rituximab leads to completely abrogation of tumor growth. This strong synergy may be explained by the induction of stress-related cytokines by chemotherapeutic agents that can effectively target cancer cells for removal by the innate immune system through macrophage infiltration and phagocytic activity,[47] potentially augmenting the described ability of daratumumab to engage ADCP.[26]

In the phase II clinical trial CARINA, LYM2001 in R/R NHL, daratumumab monotherapy did not yield the expected results in heavily pretreated FL and DLBCL patients, while no results could be concluded in MCL because of insufficient patient recruitment. However, we have identified certain NHL scenarios were daratumumab shows comparable antitumor activity as rituximab (blastic MCL) and other where exhibits superiority (transformed $CD20^{dim}$ FL). Moreover, daratumumab potentiates the antitumor activity of CHOP and R-CHOP in all three models.

In addition, as demonstrated in MM, it is likely that daratumumab may modulate the activity and frequency of CD38 expressing immune suppressive cell populations present in NHL, an effect not exerted by rituximab, and therefore may offer a superior overall antitumor effect. [29] These may be of special relevance in FL and DLBCL where infiltration of diverse T and myeloid subpopulations is specially prominent.[48] The immune-compromised mouse models used in this study preclude the analysis of this immune-modulating activity of daratumumab.

In conclusion, our findings warrant further clinical development of daratumumab in NHL providing a strong rationale for examining its clinical efficacy in different scenarios, including maintenance therapy after induction therapy, cases with anti-CD20 resistance, FL histologic transformation, and as frontline in combination with the standard of care (CHOP/ R-CHOP).

ACKNOWLEDGEMENTS

We thank Dr. Adrian Wiestner for his support with this study and his critical revision of the manuscript. Jocabed Roldan, Laura Jiménez, Sandra Cabezas and Ariadna Giro for their technical assistance. The authors would like to thank Dr J Rouquette and Ms L Teyssedre (Imaging facility, ITAV, Toulouse) for performing Daratumumab imaging within the 3D lymphoma cultures by SPIM, and Dr JJ Fournié (CRCT, Toulouse) for article comments.

FUNDING

This work was carried out at the Esther Koplowitz Center, Barcelona. Genmab and Janssen pharmaceuticals funded this research. Additional grants that contributed to this work included: Spanish Ministry of Economy and Competitiveness & European Regional Development Fund (ERDF) "Una manera de hacer Europa" for SAF2011/29326 and SAF2014/57708R to PP-G, SAF2015/31242R and SAF2015-31242-R to DC, CIBERONC (CB16/12/00334 and CB16/12/00225), the Integrated Excellence Grant from the Instituto de Salud Carlos III (ISCIII) PIE1313/00033 to EC and PP-G, and finally Generalitat de Catalunya support for AGAUR 2017SGR1009 to DC.

BIBLIOGRAPHY

1. Chihara D, Nastoupil LJ, Williams JN, Lee P, Koff JL and Fowers CR. New insights into the epidemiology of non-Hodgkin lymphoma and implications for therapy. Expert Rev Anticancer Ther. 2015;15(5):531–544.

2. Swerdlow SH, Campo E, Harris NL, et al. WHO Classification of tumours of haematopoietic and lymphoid tissues. 2008.

3. Swerdlow SH, Campo E, Pileri SA, et al. The 2016 revision of the World Health Organization (WHO) classification of lymphoid neoplasms. Blood. 2016;127(20):2375–2390.

4. Lossos IS, Gascoyne RD. Transformation of follicular lymphoma. Best Pr Res Clin Haematol. 2011;24(2):147–163.

5. Hiddemann W, Kneba M, Dreyling M, et al. Frontline therapy with rituximab added to the combination of cyclophosphamide, doxorubicin, vincristine, and prednisone (CHOP) significantly improves the outcome for patients with advanced-stage follicular lymphoma compared with therapy with CHOP alone. Blood. 2005;106(12):3725-3732.

6. Federico M, Luminari S, Dondi A, et al. R-CVP versus R-CHOP versus R-FM for the initial treatment of patients with advanced-stage follicular lymphoma: Results of the FOLL05 trial conducted by the Fondazione Italiana Linfomi. J Clin Oncol. 2013;31(12):1506–1513.

7. Kridel R, Sehn LH, Gascoyne RD. Pathogenesis of follicular lymphoma. J Clin Invest. 2012;122(10):3424–3431.

8. Alizadeh AA, Eisen MB, Davis RE, et al. Distinct types of diffuse large B-cell lymphoma identified by gene expression profiling. Nature. 2000;403(6769):503–511.

9. Tilly H, Dreyling M. Diffuse large B-cell non-Hodgkin's lymphoma: ESMO Clinical Recommendations for diagnosis, treatment and follow-up. Ann Oncol. 2009;20 Suppl 4:110-112.

10. Lim SH, Vaughan AT, Ashton-Key M, et al. Fc gamma receptor IIb on target B cells promotes rituximab internalization and reduces clinical efficacy. Blood. 2011;118(9):2530–2540.

11. Edelmann J, Gribben JG. Obinutuzumab for the treatment of indolent lymphoma. Futur Med. 2016;12(15):1769–1781.

12. Mantei K, Wood BL. Flow cytometric evaluation of CD38 expression assists in distinguishing follicular hyperplasia from follicular lymphoma. Cytom Part B Clin Cytom. 2009;76(5):315–320.

13. Pérez-Galán P, Dreyling M, Wiestner A. Mantle cell lymphoma: biology, pathogenesis, and the molecular basis of treatment in the genomic era. Blood. 2011;117(1):26–38.

14. Campo E and Rule S. Mantle cell lymphoma: evolving management strategies. Blood. 2015;125(1):48–55.

15. Dreyling M, Campo E, Hermine O, et al. Newly diagnosed and relapsed mantle cell lymphoma: ESMO Clinical Practice Guidelines for diagnosis, treatment and follow-up. Ann Oncol. 2017;28(suppl-4):iv62–iv71.

16. Cavalli F. Bortezomib-based therapy for mantle-cell lymphoma. N Engl J Med.

2015;372(23):2271.

17. Wang ML, Rule S, Martin P, et al. Targeting BTK with ibrutinib in relapsed or refractory mantle-cell lymphoma. N Engl J Med. 2013;369(6):507–516.

18. Martin P, Maddocks K, Leonard JP, et al. Postibrutinib outcomes in patients with mantle cell lymphoma. Blood. 2016;127(12):1559–1663.

19. Orchard J, Garand R, Davis Z, et al. A subset of t(11; 14) lymphoma with mantle cell features displays mutated IgV H genes and includes patients with good prognosis, nonnodal disease. Blood. 2003;101(12):4975–4981.

20. Camacho FI, Algara P, Rodríguez A, et al. Molecular heterogeneity in MCL defined by the use of specific V H genes and the frequency of somatic mutations. Blood. 2003;101(10):4042–4046.

21. Pérez-Galán P, Mora-Jensen H, Weniger MA, et al. Bortezomib resistance in mantle cell lymphoma is associated with plasmacytic differentiation. Blood. 2011;117(2):542–553.

22. Deaglio S, Vaisitti T, Aydin S, Ferrero E, Malavasi F. In-tandem insight from basic science combined with clinical research: CD38 as both marker and key component of the pathogenetic network underlying chronic lymphocytic leukemia. Blood. 2006;108(4):1135–1144.

23. McKeage K. Daratumumab: First Global Approval. Drugs. 2016;76(2):275–281.

24. https://www.accessdata.fda.gov/drugsatfda_docs/label/2017/761036s005lbl.pdf. *Janssen Biotech Inc. DarzalexTM (daratumumab): prescribing information* 2017;1–29.

25. de Weers M, Tai Y-T, van der Veer MS, et al. Daratumumab, a novel therapeutic human CD38 monoclonal antibody, induces killing of multiple myeloma and other hematological tumors. J Immunol. 2011;186(3):1840–1848.

26. Overdijk MB, Verploegen S, Bögels M, et al. Antibody-mediated phagocytosis contributes to the anti-tumor activity of the therapeutic antibody daratumumab in lymphoma and multiple myeloma. MAbs. 2015;7(2):311–320.

27. Overdijk MB, Jansen JHM, Nederend M, et al. The therapeutic CD38 monoclonal antibody daratumumab induces programmed cell death via Fcγ Receptor-mediated cross-linking. J Immunol. 2016;197(3):807-813.

28. Lammerts van Bueren J, Jakobs D, Kaldenhoven N, et al. Direct in Vitro Comparison of Daratumumab with Surrogate Analogs of CD38 Antibodies MOR03087, SAR650984 and Ab79 [abstract]. Blood. 2014;124(21):Abstract 3474.

29. Krejcik J, Casneuf T, Nijhof IS, et al. Daratumumab depletes CD38+ immune-regulatory cells, promotes T-cell expansion, and skews T-cell repertoire in multiple myeloma. Blood. 2016;128(3):384–394.

30. Matas-Céspedes A, Vidal-Crespo A, Rodriguez V, et al. The human CD38 monoclonal antibody daratumumab shows antitumor activity and hampers leukemia-microenvironment interactions in chronic lymphocytic leukemia. Clin Cancer Res. 2017;23(6):1493–1505.

31. Krejcik J, van de Donk NWCJ. Trogocytosis represents a novel mechanism of action of daratumumab in multiple myeloma. Oncotarget. 2018;9(72):33621–33622.

32. Krejcik J, Frerichs KA, Nijhof IS, et al. Monocytes and Granulocytes Reduce CD38

Expression Levels on Myeloma Cells in Patients Treated with Daratumumab. Clin Cancer Res. 2017;23(24):7498–7511.

33. Eder T, Eder IE. 3D Hanging Drop Culture to Establish Prostate Cancer Organoids. In: Koledova Z, editor. 3D Cell Culture: Methods and Protocols. New York, NY: Springer New York; p167–175.

34. Decaup E, Jean C, Laurent C, et al. Anti-tumor activity of obinutuzumab and rituximab in a follicular lymphoma 3D model. Blood Cancer J. 2013;9(3):131.

35. Matas-Céspedes A, Rodriguez V, Kalko SG, et al. Disruption of follicular dendritic cells-follicular lymphoma cross-talk by the pan-PI3K inhibitor BKM120 (Buparlisib). Clin Cancer Res. 2014;20(13):3458–3471.

36. Moros A, Rodríguez V, Saborit-Villarroya I, et al. Synergistic antitumor activity of lenalidomide with the BET bromodomain inhibitor CPI203 in bortezomib-resistant mantle cell lymphoma. Leukemia. 2014;28(10):2049–2059.

37. Campbell KS, Hasegawa J. Natural killer cell biology: an update and future directions. J Allergy Clin Immunol. 2013;132(3):536–544.

38. Chao MP, Alizadeh AA, Tang C, et al. Anti-CD47 Antibody Synergizes with Rituximab to Promote Phagocytosis and Eradicate Non-Hodgkin Lymphoma. Cell. 2010;142(5):699–713.

39. Golay J, Lazzari M, Facchinetti V, et al. CD20 levels determine the in vitro susceptibility to rituximab and complement of B-cell chronic lymphocytic leukemia: further regulation by CD55 and CD59. Blood. 2001;98(12):3383–3389.

40. Vidal L, Gafter-Gvili A, Dreyling MH, et al. Maintenance Therapy for Patients with Mantle Cell Lymphoma (MCL) - a Systematic Review and Meta-Analysis of Randomized Controlled Trials (RCTs). Blood. 2016;128(22):1802.

41. Vidal L, Gafter-Gvili A, Salles G, et al. Rituximab maintenance improves overall survival of patients with follicular lymphoma-Individual patient data meta-analysis. Eur J Cancer. 2017;76216–76225.

42. Foran JM, Norton AJ, Micallef IN, et al. Loss of CD20 expression following treatment with rituximab (chimaeric monoclonal anti-CD20): A retrospective cohort analysis. Br J Haematol. 2001;114(4):881–883.

43. Beers SA, French RR, Chan HT, et al. Antigenic modulation limits the efficacy of anti-CD20 antibodies: Implications for antibody selection. Blood. 2010;115(25):5191–5201.

44. Beum PV, Peek EM, Lindorfer MA, et al. Loss of CD20 and bound CD20 antibody from opsonized B cells occurs more rapidly because of trogocytosis mediated by Fc receptor-expressing effector cells than direct internalization by the B cells. J Immunol. 2011;187(6):3438–3447.

45. Elhassadi E, Murphy M, Hacking D, Farrell M. Durable treatment response of relapsing CNS plasmacytoma using intrathecal chemotherapy, radiotherapy, and Daratumumab. Clin Case Rep. 2018;6(4):723–728.

46. Touzeau C, Moreau P. How I treat extramedullary myeloma. Blood. 2016;127(8):971–976.

47. Pallasch CP, Leskov I, Braun CJ, et al. Sensitizing protective tumor microenvironments to antibody-mediated therapy. Cell. 2014;156(3):590–602.

48. Tosolini M, Algans C, Pont F, Ycart B Fournié JJ. Large-scale microarray profiling reveals four stages of immune escape in non-Hodgkin lymphomas. Oncoimmunology. 2016;5(7):e1188246.

Table 1

Cell line	NHL subtype[1]	CD38 sABC[2]	%CD38[1]	MFIR CD38[3]	%CD20[1]	MFIR CD20[3]	%CD46[1]	%CD55[1]	%CD59[1]	%ADCC[4]	%ADCP[4]	%CDC[4]
Jeko	MCL	16253	84	22	100	46	92	98	61	58	41	7
REC-1	MCL	106234	100	155	100	77	99	99	88	60	46	18
HBL2	MCL	25317	100	92	100	99	98	96	98	28	21	0
Mino	MCL	127458	100	51	100	42	97	100	96	32	35	0
UPN1	MCL	54089	99	97	97	8	98	99	63	36	73	0
Z138	MCL	186239	100	120	100	28	100	75	69	53	89	0
DOHH2	FL	22369	87	20	99	31	100	76	98	25	38	0
SC-1	FL	71726	100	40	32	4	95	96	83	41	81	1
RL	FL	132684	96	76	93	49	100	94	97	52	45	6
WSU-FSCCL	FL	89707	97	354	8	2	82	81	94	67	92	7
Toledo	DLBCL	123539	99	186	89	13	94	99	97	34	50	14
WSU-DLCL2	DLBCL	14926	94	46	99	137	95	95	98	45	15	1
SU-DHL-6	DLBCL	174033	92	383	98	172	97	44	31	64	56	5
SU-DHL-4	DLBCL	96623	96	108	100	45	93	45	95	61	34	8
Daudi	BL	415667	100	276	99	30	88	17	9	63	79	96

[1]Percentage of positive cells for CD38, CD20, CD46, CD55 and CD59 determined by flow cytometry, referred to isotype control; [2]sABC: number of surface antibodies bound per cell evaluated by QuantiBRITE™ CD38-PE; [3]MFIR: mean fluorescence ratio referred to isotype control; [4]Percentage of ADCC and ADCP induction at 1 µg/mL DARA. Percentage of CDC induction at 10 µg/mL DARA.

FIGURE LEGENDS

Figure 1. Daratumumab induces ADCC and ADCP in the presence of external effectors in NHL.

(A) MCL, (B) FL, and (C) DLBCL cell lines were treated with increasing DARA doses (0.0001-1 µg/mL) in the presence of PBMCs from healthy donors at a E:T ratio of 50:1 for 4 hours. Viability was then evaluated by calcein release assay. The BL cell line, Daudi, was included as positive control. (D) MCL, (E) FL, and (F) DLBCL cell lines were labeled with calcein and incubated for 4h with the mΦ at an E:T ratio of 1:1 in the presence of a fixed DARA concentration of 1 µg/mL, followed by flow cytometry analysis in triplicates. ADCP was calculated as the percentage of $CD19^+$ $calcein^+$ $F4/80^-$ cells after DARA treatment referred to isotype-treated cells. Daudi cells were included as positive control.

Figure 2. Daratumumab effect in a 3D model of FL.

3D spheroids of RL-GFP cells were obtained after 3 days of culture in hanging drop plates or 96-well ultra-low attachment plates, and then treated with 10 µg/mL of Isotype control (IgG1), or 1 or 10 µg/mL of DARA at different times. (A) 3D reconstruction images produced by SPIM; fluorescence was measured at a λ_{ex} of 488nm (GFP) and 561nm (mAbs labeling). (B) Percentage of mAb diffusion, representing quantity of the mAb in the spheroid. (C) Percentage of mAb penetration, representing maximum depth of the mAb in the spheroid. (D) Spheroid volume (mm^3) time course (n = number of spheroids per treatment). Statistical differences between groups were assessed by unpaired *t*-test (**, $p < 0.01$; ***, $p < 0.001$).

Figure 3. Daratumumab efficacy in pre-emptive models of MCL and tFL. $10x10^6$ REC-1 cells (A) or RL-luc cells (B) were mixed with matrigel (1:1) and subcutaneously injected in SCID mice (n = 6 per group). Animals received one dose every other week (10 mg/kg of isotype control (IgG1) or DARA) starting the day of cell inoculation. Tumor growth curves over time clearly show total regression was achieved in both models. As RL cell line expressed the luciferase gene, sequential bioluminescence images were captured at different time points (B). Statistical differences between groups were assessed by unpaired *t*-test (***, $p < 0.001$).

Figure 4. Daratumumab monotherapy in a systemic model of MCL and FL compared to rituximab. $10x10^6$ Z-138 (MCL) and WSU-FSCCL (FL) cells were intravenously injected in SCID mice (n = 10 per group). Treatment (isotype control (IgG1)/ Daratumumab/ Rituximab) started one week after inoculation and went on weekly for 4 weeks (20/10/10/10 mg/kg), as indicated by the red arrows. Mice were monitored twice weekly for any sign of disease and were euthanized when body weight decreased 15-20%. Survival curves are represented. Statistical

differences between groups were assessed by log-rank test**. Z-138** : Overall significance***p < 0.001; Isotype; Ctrl vs DARA ***p < 0.01; DARA vs Rituximab ns p=0.2907. **WSU-FSCCL**: Overall significance ***p < 0.001; Isotype Ctrl vs Dara ***p ≤ 0.001; Dara vs Rituximab *p=0.045.

Figure 5. Daratumumab combined with R-CHOP in MCL and tFL. $10x10^6$ REC-1 (A-B) and RL-luc (C-D) cells were mixed with matrigel (1:1) and subcutaneously injected in SCID mice (REC-1: n=5-7 per group; RL: n 7-10 per group). Treatment as monotherapy (isotype control (IgG1)/ DARA/ RITUX/ CHOP) or the combination regimen DARA ± RITUX ± CHOP started one week after inoculation and went on weekly during 3 weeks for the mAbs (20/10/10 mg/kg) in REC model, and 4 weeks (20/10/10/10 mg/kg) for RL model. CHOP was given as an initial unique dose the first day of treatment in both models. Tumor growth curves over time are represented for each cohort (A and C). Tumor weight for each treatment was averaged and represented at endpoint for REC-1 (B) and RL models (D). Statistical differences between groups were assessed by unpaired *t*-test (**, p < 0.01; ***, p < 0.001).

Figure 6. Daratumumab combined with R-CHOP in a patient-derived DLBCL xenograft model. Fragments from a patient-derived DLBCL were injected subcutaneously into SCID mice (n = 8-10) and staged to approximately 150 to 250 mm^3 mean tumor volume to measure (A) tumor growth and (B) OS. 20 mg/kg daratumumab was administered weekly alone or in combination with CHOP (20 mg/kg cyclophosphamide, 1.25 mg/kg doxorubicin, 0.2 mg/kg vincristine, and 0.15 mg/kg prednisone) or R-CHOP (10 mg/kg rituximab+ CHOP) for a total of three weeks.

Figure 1

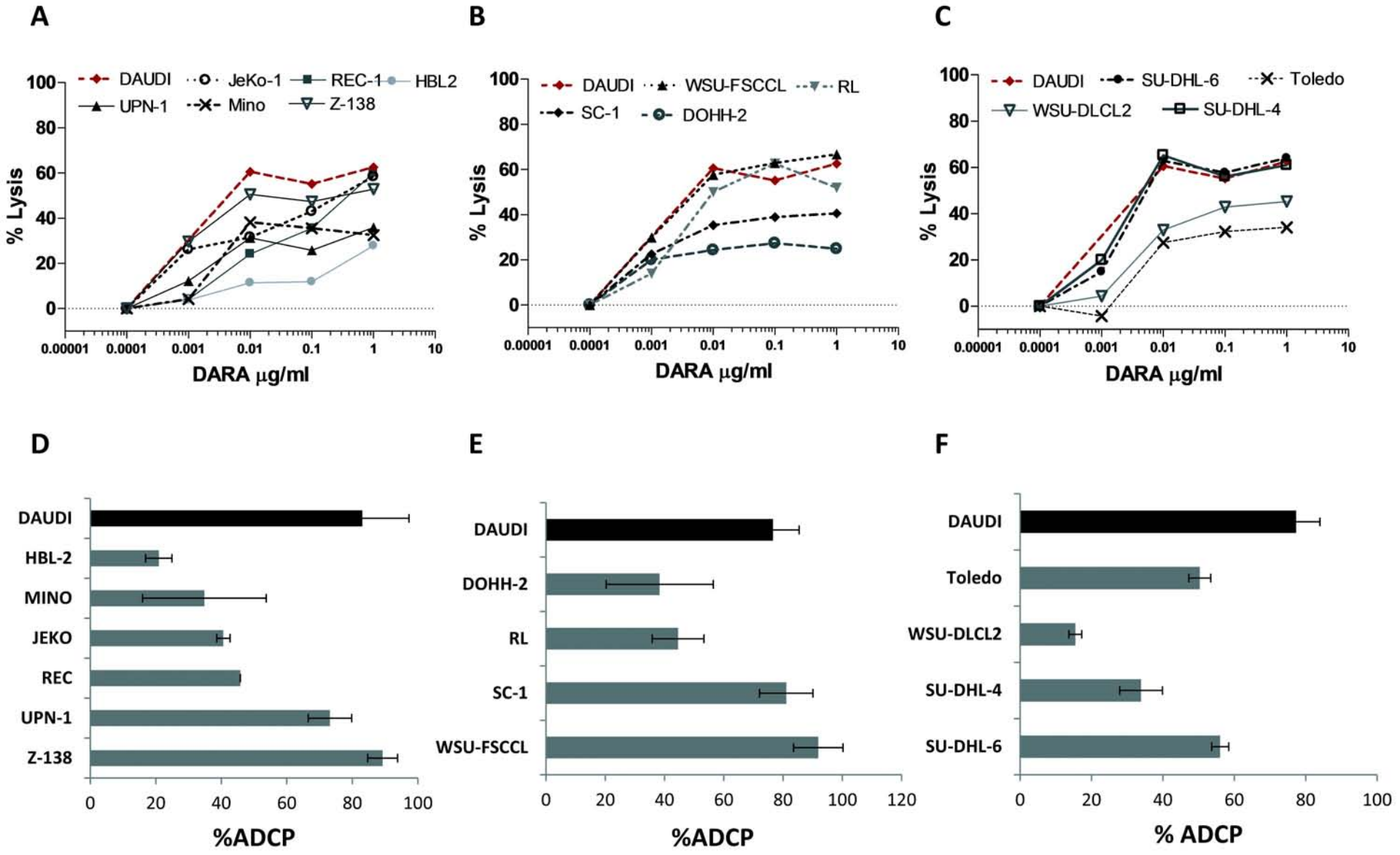
A
DAUDI
JeKo-1
REC-1
HBL2
UPN-1
Mino
Z-138
% Lysis
DARA μg/ml
B
DAUDI
WSU-FSCCL
RL
SC-1
DOHH-2
% Lysis
DARA μg/ml
C
DAUDI
SU-DHL-6
Toledo
WSU-DLCL2
SU-DHL-4
% Lysis
DARA μg/ml
D
DAUDI
HBL-2
MINO
JEKO
REC
UPN-1
Z-138
%ADCP
E
DAUDI
DOHH-2
RL
SC-1
WSU-FSCCL
%ADCP
F
DAUDI
Toledo
WSU-DLCL2
SU-DHL-4
SU-DHL-6
% ADCP

Figure 2

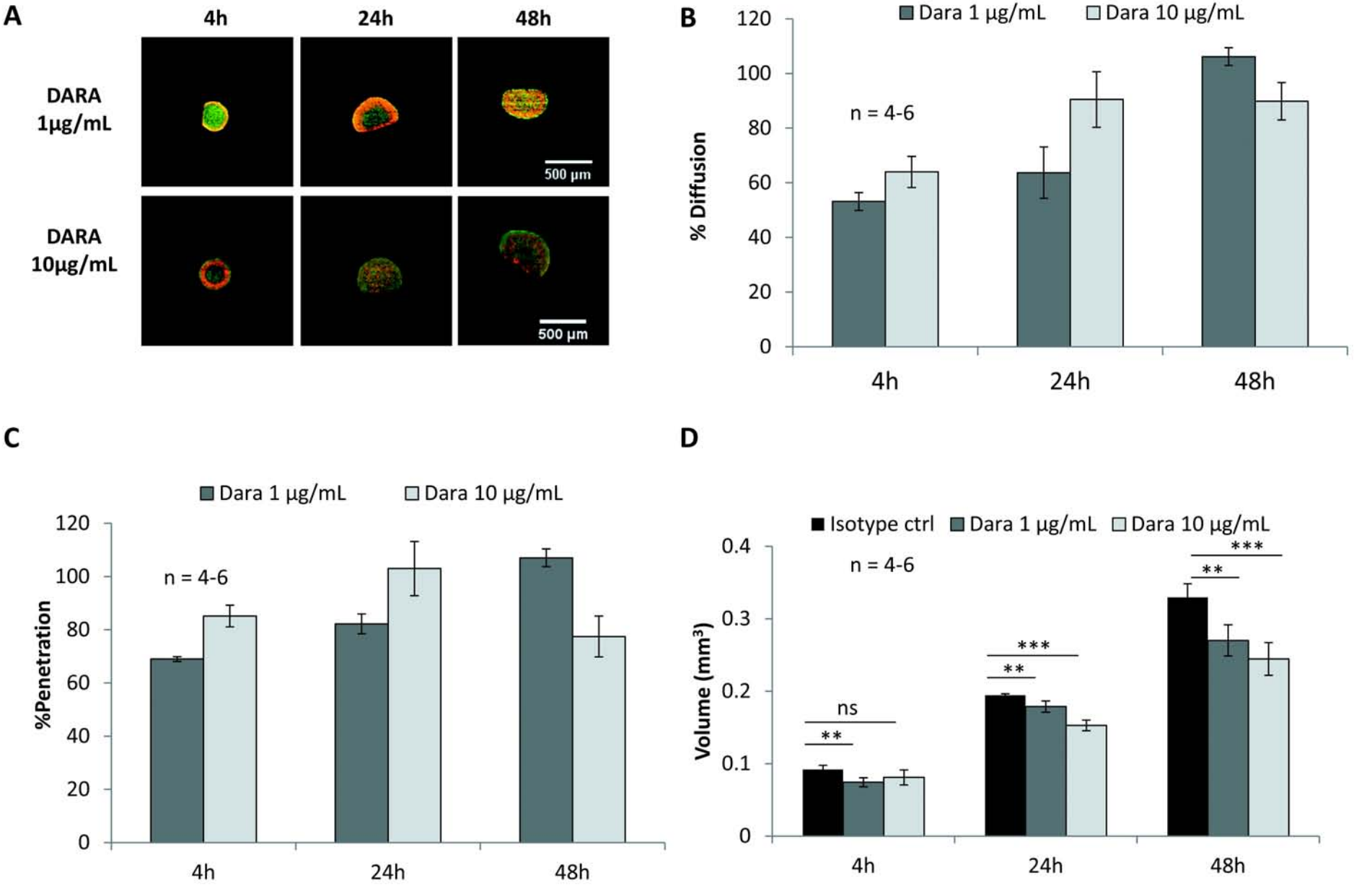
A
4h
24h
48h
DARA 1µg/mL
DARA 10µg/mL
500 µm
500 µm
B
Dara 1 µg/mL
Dara 10 µg/mL
% Diffusion
n = 4-6
4h
24h
48h
C
Dara 1 µg/mL
Dara 10 µg/mL
%Penetration
n = 4-6
4h
24h
48h
D
Isotype ctrl
Dara 1 µg/mL
Dara 10 µg/mL
Volume (mm³)
n = 4-6
ns
**
***
**
***
**
4h
24h
48h

Figure 3

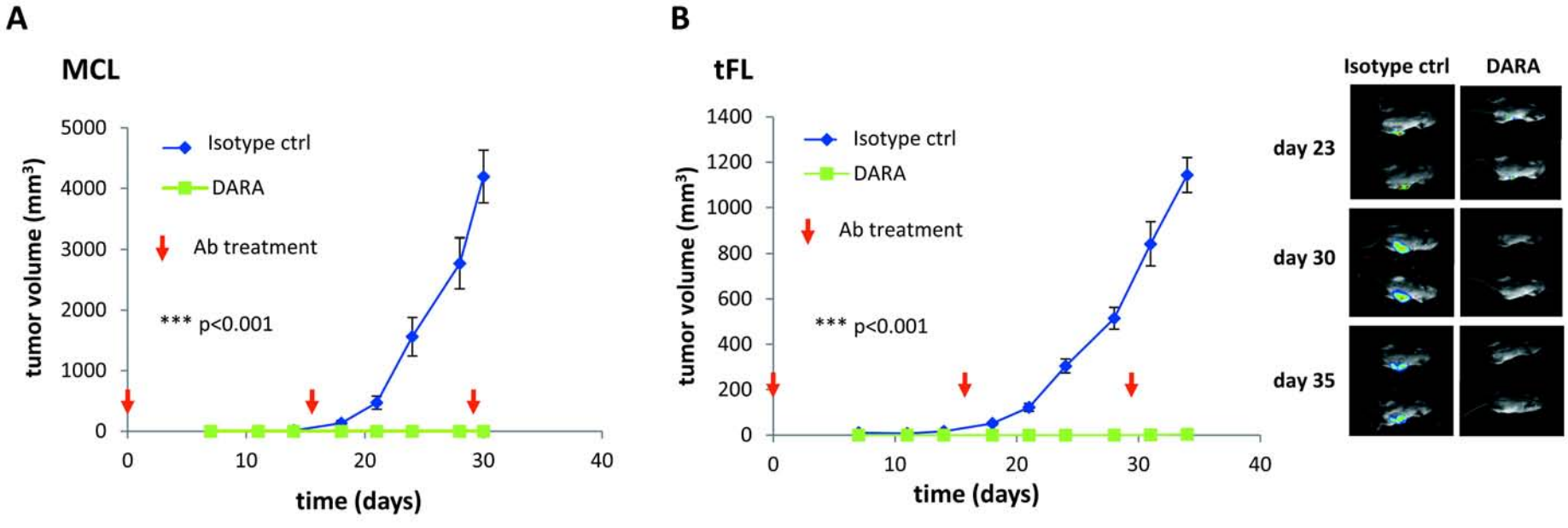
A
MCL
tumor volume (mm³)
5000
4000
3000
2000
1000
0
Isotype ctrl
DARA
Ab treatment
*** p<0.001
0
10
20
30
40
time (days)
B
tFL
tumor volume (mm³)
1400
1200
1000
800
600
400
200
0
Isotype ctrl
DARA
Ab treatment
*** p<0.001
0
10
20
30
40
time (days)
Isotype ctrl
DARA
day 23
day 30
day 35

Figure 4

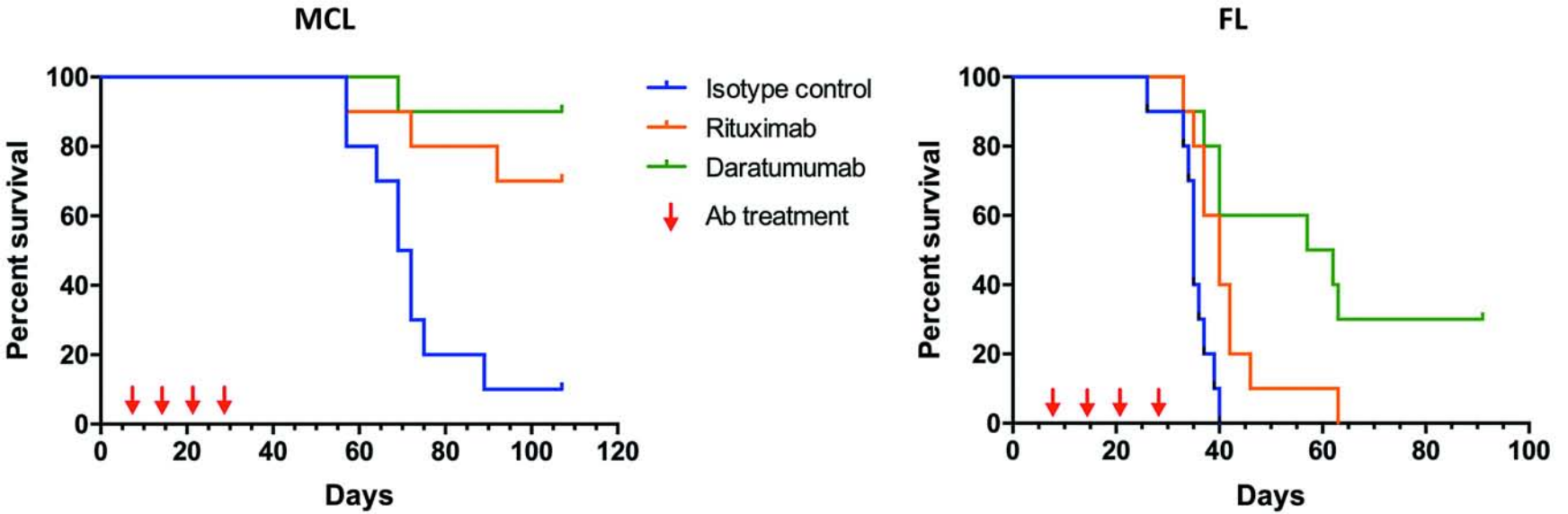
MCL
Percent survival
100
80
60
40
20
0
0
20
40
60
80
100
120
Days
Isotype control
Rituximab
Daratumumab
Ab treatment
FL
Percent survival
100
80
60
40
20
0
0
20
40
60
80
100
Days

Figure 5

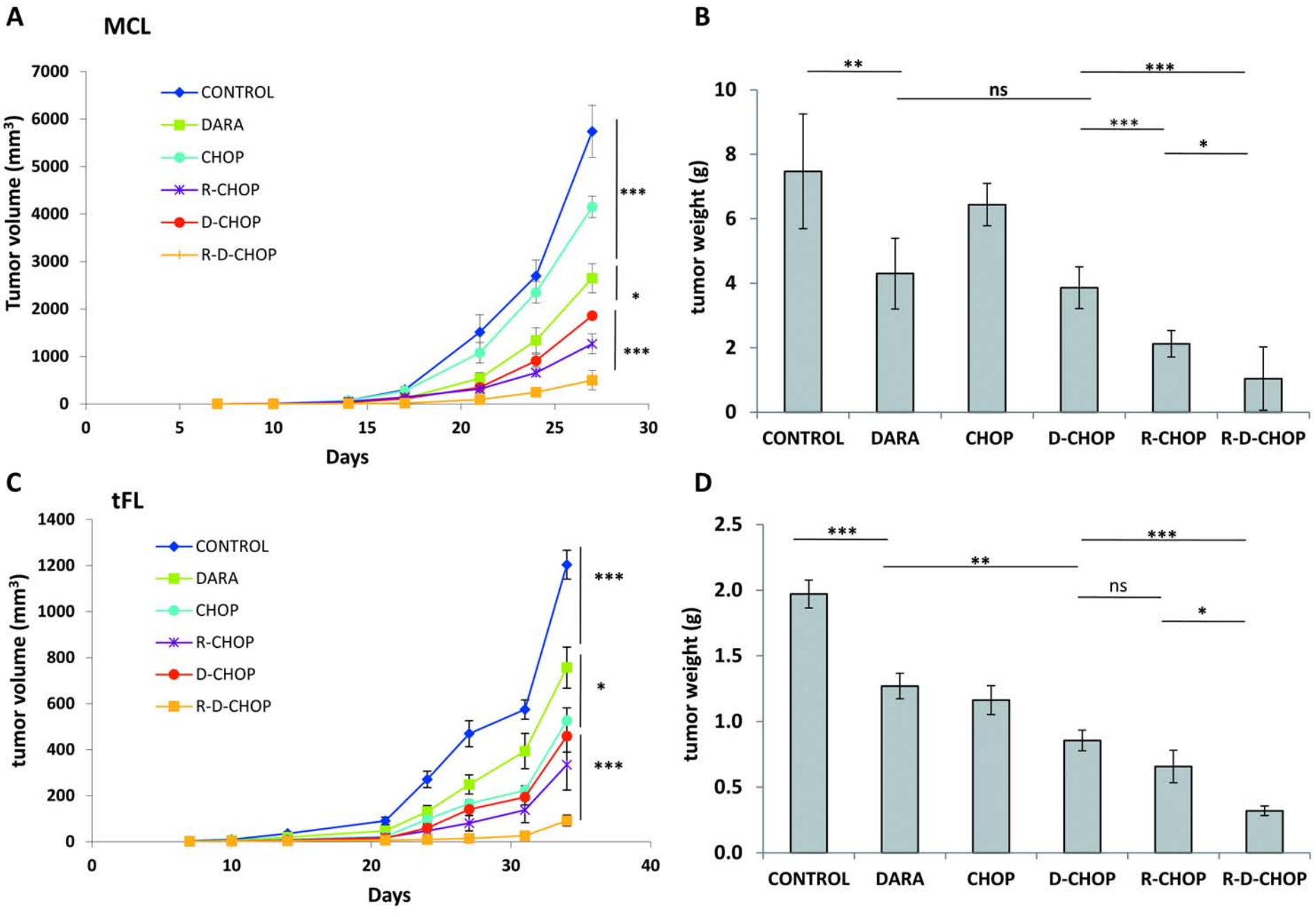
A
MCL
Tumor volume (mm³)
Days
CONTROL
DARA
CHOP
R-CHOP
D-CHOP
R-D-CHOP
***
*
***
B
tumor weight (g)
**
ns
***
***
*
CONTROL
DARA
CHOP
D-CHOP
R-CHOP
R-D-CHOP
C
tFL
tumor volume (mm³)
Days
CONTROL
DARA
CHOP
R-CHOP
D-CHOP
R-D-CHOP
***
*
***
D
tumor weight (g)
***
**
ns
***
*
CONTROL
DARA
CHOP
D-CHOP
R-CHOP
R-D-CHOP

Figure 6

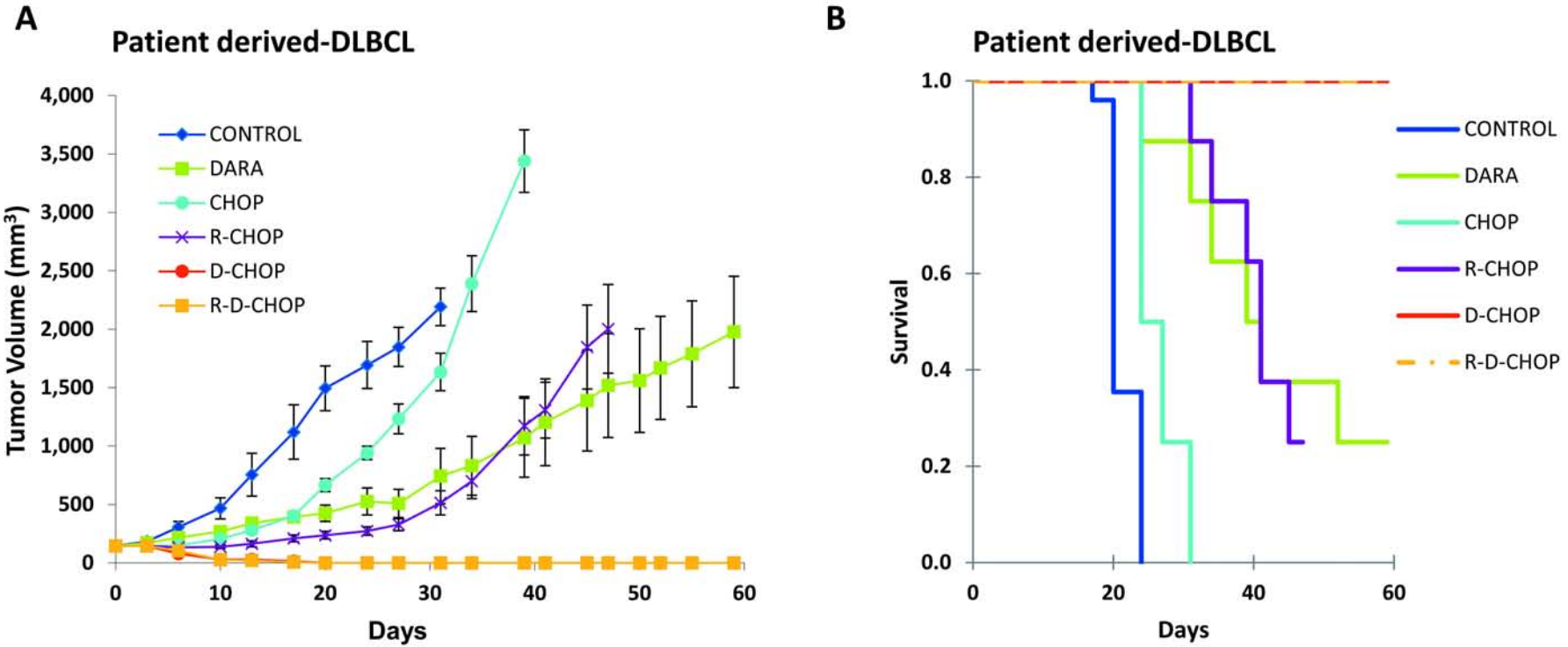
A
Patient derived-DLBCL
Tumor Volume (mm³)
4,000
3,500
3,000
2,500
2,000
1,500
1,000
500
0
0
10
20
30
40
50
60
Days
CONTROL
DARA
CHOP
R-CHOP
D-CHOP
R-D-CHOP
B
Patient derived-DLBCL
Survival
1.0
0.8
0.6
0.4
0.2
0.0
0
20
40
60
Days
CONTROL
DARA
CHOP
R-CHOP
D-CHOP
R-D-CHOP

SUPPLEMENTARY INFORMATION

SUPPLEMENTAL METHODS

Cell lines

FL cell lines DOHH-2, RL, SC-1, WSU-FSCCL as well as the Burkitt lmphoma (BL) Daudi cell line and DLBCL cell lines SU-DHL-4 and SU-DHL-6 were obtained from DSMZ (Braunschweig, Germany). MCL cell lines Jeko-1, Mino, REC-1, Z-138 and DLBCL cell line WSU-DLCL2 were obtained from ATCC (LGC Standards, Teddington, UK). HBL-2 was kindly provided by Prof. M Dreyling (University Hospital, Munich, Germany), UPN-1 by Dr. A Turhan (Hôpital Bicêtre et Paul Brousse, Villejuif, France) and Toledo cell line by Dr. MA Piris (Fundación Jiménez Díaz, Madrid, Spain). The RL cell line expressing luciferase (RL-luc) was generated *via* retroviral transduction. Retroviral vectors containing full-length pLHCX-luc were kindly provided by Dr. Bofill-De Ros (IDIBAPS, Barcelona, Spain) (see below method description). RL-GFP cells were produced by the Inserm UMR1037 vector facility (CRCT, Toulouse, France) and provided by JJ Fournié's laboratory (CRCT). Cell lines were cultured in RPMI-1640 supplemented with 10% FBS, 2 mmol/L L-glutamine, 50 µg/mL penicillin/streptomycin (Life Technologies) and were maintained in a humidified atmosphere at 37ºC containing 5% CO_2. Normocin (100 µg/mL; InvivoGen) was added to the cell line cultures to prevent mycoplasma contamination in cell lines that were routinely tested for mycoplasma infection by PCR. The identity of all cell lines was verified by using the AmpFISTR identifier kit (Life Technologies).

Retroviral transfection of NHL cells

Supernatant of Phoenix cells containing retroviral particles was used to infect RL cells by centrifugation (2500 rpm for 90 minutes) in the presence of polybrene (Sigma Aldrich). Selection of transfected cells was started 2 days after infection with 200 µg/mL of hygromycin B (Sigma Aldrich). The Luciferase Assay System kit (Promega) was used to confirm expression of the luciferase gene, following the manufacturer's instructions.

Antibody-dependent cellular cytotoxicity

ADCC was performed using a calcein-release assay as described previously (30). Target cells were exposed to 10-fold serial dilutions of either isotype control (CNTO 3930, spontaneous release) or daratumumab (range, 1 to 0.0001 µg/mL) in RPMI-1640 in the presence of healthy donor PBMC at E:T ratio of 50:1 for 4 hours. 10% Triton was used to determine maximal release. The percentage of cellular cytotoxicity was calculated using the following formula:

$$\%\ specific\ lysis\ = 100 \times \frac{experimental\ release(RFU) - spontaneous\ release\ (RFU)}{maximal\ release(RFU) - spontaneous\ release\ (RFU)}$$

Antibody-dependent cellular phagocytosis

ADCP was carried out with macrophages generated from monocytes isolated from BM of the hind legs of female SCID mice (C.B-17/Icr-Prkdc^{scid}/Crl; Janvier Labs), by flushing the femurs. The cells were cultured for 7 days in DMEM supplemented with 10% FBS, 2 mM L-glutamine, 50 µg/mL penicillin/streptomycin, and 50 U/ml M-CSF (Cell Guidance), and the culture medium was renewed every 3 days. On day 7, mϕ were detached with 0.1% trypsin-EDTA and characterized by flow cytometry (CD11b^{+}, F4/80^{+}) (mouse antibodies obtained from eBiosciences and Invitrogen, respectively). The mϕ were seeded at 2.5×10^{5} cells per well into non-tissue cultured treated 24-well plates and allowed to adhere overnight. Target cells were labeled with 0.01µM Calcein-AM and added to the mϕ at an E:T ratio of 1:1 in the presence of a fixed mAb concentration of either isotype control (CNTO 3930) or daratumumab at 1 µg/mL. After 4hr of incubation, the non-phagocytosed target cells were collected.The mϕ were detached with 0.1% trypsin-EDTA, added to the non-phagocytosed target cells and stained for F4/80 expression.The amount of remaining target cells (CD19^{+} calcein^{+} F4/80^{-}) was determined on an Attune acoustic cytometer. The percentage of killed target cells in the presence of daratumumab compared with isotype control was calculated using the following formula:

$$\%\ ADCP = 100 - [100 \times \frac{remaining\ target\ cells\ after\ DARA\ treatment}{remaining\ target\ cells\ \ after\ isotype\ control\ treatment}]$$

Complement-dependent cytotoxicity

Target cells were labeled with 1 µM Calcein-AM (Life Technologies) for 30 min at 37ºC. Afterwards, cells were washed thrice with PBS, plated in triplicate at 1×10^{5} cells/well in 96-well round bottom plates, and preincubated (room temperature {RT}, 15 min) with 10-fold serial dilutions of either isotype control (CNTO 3930) or DARA (range: 10 to 0.01 µg/mL) in RPMI 1640. Culture medium was added instead of mAb to determine the spontaneous calcein release and 1% Triton X-100 was used to determine the maximal calcein release. Thereafter, 10% normal human AB serum was added and incubated for 45 min at 37°C. The plates were centrifuged, supernatants transferred into black plates (Thermo Scientific) and fluorescence measured in a Synergy spectrophotometer (Bio-Tek) (excitation filter: 485 ± 20 nm; band-pass filter: 530 ± 20 nm). The percentage of cellular cytotoxicity was calculated using the following formula:

$$\%\ specific\ lysis\ = 100 \times \frac{experimental\ release(RFU) - spontaneous\ release\ (RFU)}{maximal\ release(RFU) - spontaneous\ release\ (RFU)}$$

3D lymphoma cultures and Selective Plane Illumination Microscopy (SPIM) analysis

Multicellular aggregates of lymphoma cells were generated by the hanging drop method. RL-GFP cells (2.5x10^5 cells/mL) were prepared in complete medium containing 1% Methocult (STEMCELL Technologies), 40 µL of this suspension were pipetted into each well of the Perfecta3D® hanging drop plates (Sigma-Aldrich). After 72 hours of incubation, spheroids were transferred to 96 well plates and treated for 4, 24 and 48 hours with isotype or daratumumab labeled in red with the Mix-n-Stain™CF™ 555 Antibody Labeling Kit (Sigma-Aldrich), then fixed with 4% paraformaldehyde (Sigma-Aldrich) and analyzed by SPIM. Antibody penetration and diffusion were determined according to the following formulas:

$$\%\ penetration\ = 100 \times \frac{Global\ volume\ 561\ nm}{Real\ volume\ 488\ nm}$$

$$\%\ diffusion\ = 100 \times \frac{Real\ volume\ 561\ nm}{Real\ volume\ 488\ nm}$$

Volumes were measured after imaging on an inverted microscope according to the formula:

$$volume\ = \frac{4}{3} \times \pi \times L\ (longest\ diameter) \times l^2 (shortest\ diameter)$$

CD38 molecules per cell quantification

FL and MCL cell lines were stained with QuantiBRITE™ CD38-PE (BD Biosciences) and the mean fluorescence intensities were assessed in an Attune acoustic focusing cytometer (Life Technologies). The specific Antibody Binding Capacity (sABC) was calculated by interpolation in a linear regression curve obtained by QuantiBRITE™ PE Beads (BD Biosciences).

Systemic mouse models

SCID mice were intravenously (iv) injected with 10x10^6 WSU-FSCCL (FL) or Z-138 cells (MCL), following approval of the protocol by the Animal Testing Ethic committee of the University of Barcelona and Generalitat de Catalunya (Protocol # 9971). One week later, mice were randomly assigned into cohorts of 10 mice per group and received one intraperitoneal injection of 20 mg/kg of daratumumab, or rituximab or isotype control on day 7, and thereafter 10 mg/kg weekly for 3 weeks (20/10/10/10 schedule). Mice were monitored twice weekly and sacrificed if they have lost 15% to 20% of weight and/or showed signs of disease. The presence of tumor cells was evaluated first macroscopically and then by flow cytometry. Cells from infiltrated organs were obtained by tissue homogenization. BM cells were obtained after flushing the femoral and tibia bones with RPMI-1640 media. These samples were filtered

through 70 μm nylon sieves (BD Falcon). Erythrocytes were lysed using ACK buffer (Quality Biological Inc.), followed by staining with huCD45/CD19/CD10 antibodies, for the WSU-FSCCL model; or huCD45/CD19 antibodies for the Z-138 model, and analysis by flow cytometer under constant flow rate in an Attune acoustic focusing cytometer (Life Technologies).

In vivo daratumumab combinations in MCL and FL subcutaneous mouse models

SCID mice were subcutaneously (sc) injected with $10x10^6$ RL-luc cells in the FL model or $10x10^6$ REC-1 cells in the MCL model. Mice were randomly assigned into cohorts of 6-8 mice and treated once a week ip with the isotype control, daratumumab, or rituximab, starting when tumors were palpable (day 7) following the schedule (20/10/10 mg/kg in REC-1 and 20/10/10/10 mg/kg in RL-luc). The chemotherapy regimen CHOP was given as an initial single dose with the first dose of antibodies (cyclophosphamide: 25mg/kg; doxorubicin: 2.5mg/kg; vincristine: 0.4mg/kg prednisone: 0.15mg/kg). Tumor volume was measured twice per week with external calipers and calculated using the standard formula: $s^2 \times l \times 0.5$, where (s) is the shortest diameter of the tumor and (l) the longest. As the RL cell line expressed the luciferase gene, sequential bioluminescence images were captured after injecting 150 mg/kg XenoLight D-Luciferin (Perkin Elmer), and measured radiance by Wasabi software (Hamamatsu Photonics). Animals were sacrificed after one month according to institutional guidelines, and tumors were collected and weighed. Tumor samples were formalin-fixed and embedded in paraffin. When indicated, tissue sections were stained with H&E, phosho-histone H3 (pH3) (Epitomics) or CD31 (Santa Cruz Biotechnology) followed by evaluation on an Olympus DP70 microscope using Cell B Basic Imaging Software (Olympus).

SUPPLEMENTAL FIGURE LEGENDS

Figure S1. Correlation between the number of CD38 molecules per cell and effector mediated cell death. Number of surface antibodies bound per cell (sABC) of CD38 was quantified in MCL, FL and DLBCL cell lines, including Daudi as a positive control, and plotted for correlation with (A) ADCC and (B) ADCP induction by DARA at 0.1 μg/mL and 1 μg/mL, respectively. Statistical significance was assessed by Spearman test.

Figure S2. Daratumumab decreases CD38 surface expression in the presence of macrophages. ADCP was performed in representative MCL, FL and DLBCL cell lines. At the end point (4hr) CD38 surface expression was evaluated in the non-phagocytosed cells using an antibody compatible with daratumumab (HuMax-003 FITC) provided by Janssen. *p* values were calculated using two-way ANOVA.

Figure S3. Daratumumab exerts a direct effect in 3D lymphoma models. 2500 cells from MCL, FL and DLBCL cells lines were seeded on ultra-low attachment plates (ULA) at day 0 and daratumumab (10μg/mL) was added at 3 day for 48hr. Images were captured in a Cytation 1 Imaging system (Biotek) using x4 magnification and Hoechst counterstained (A). Spheroids were measured using Gen5 software and the was volume estimated by the formula (B):

$$volume \ = \frac{4}{3} \times \pi \times L\ (longest\ diameter) \times l^2 (shortest\ diameter)$$

Afterwards, these spheroids were manually disaggregated and cell count was evaluated by flow cytometry (C).

Figure S4. Tumor infiltration in systemic xenograft models of FL and MCL. (A-B) Tumor cells infiltrating the brain, BM, spleen and lungs from the Z138 model were recovered at the endpoint, stained with huCD45/CD19 and counted by flow cytometry. Representative density plots for one mouse of each cohort are shown. (C and D) Total number of huCD45$^+$/CD19$^+$/CD10$^+$ cells from the WSU-FSCCL model were recovered from the brain, spleen and BM of the different treatments and enumerated by flow cytometry. Representative density plots for one mouse of each cohort are shown. Statistical differences between groups were assessed by unpaired *t*-test (*, $p < 0.05$; **, $p < 0.01$; ***, $p < 0.001$). CT = isotype control

Figure S5. Daratumumab combined with R-CHOP in tFL. The experimental set up was the one described in figure 5 C-D. (A) Bioluminescence images were captured at endpoint. Representative images of 2 mice from each group are shown as an example of tumor burden. (B) Bioluminescent signal was quantified, and photon emission is represented as the mean of photons/s in 2 mice from each group. (C) IHC staining of H&E, pH3 and CD31 were assessed in representative tumors from each treatment (magnification, 200x).

Figure S6. CD38 expression of DLBCL patient derived xenograft. CD38 expression was assessed by IHC in a tissue section of ST1361 DLBCL patient biopsy

Figure S1

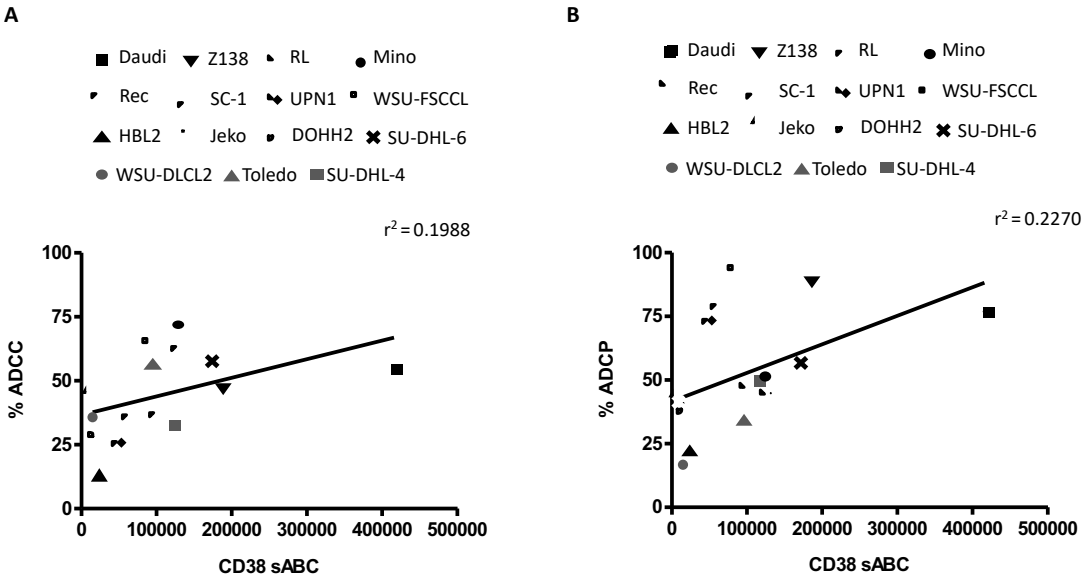

Figure S2

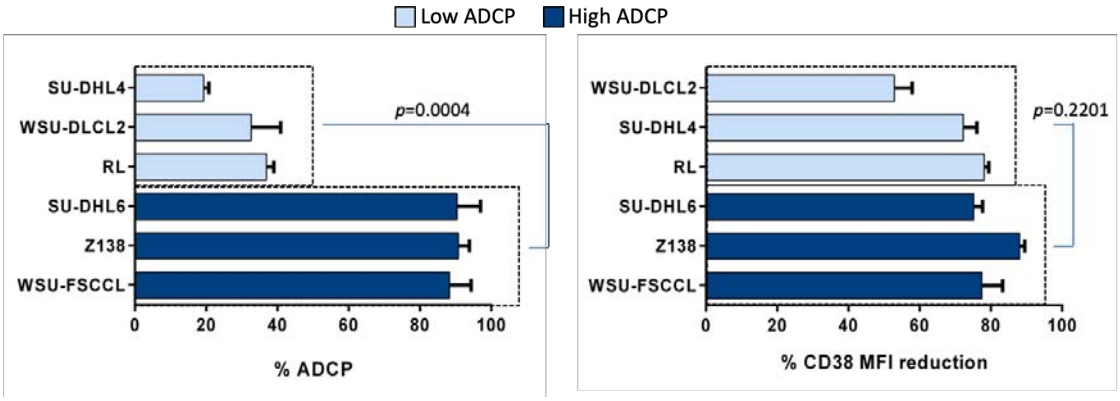

Figure S3

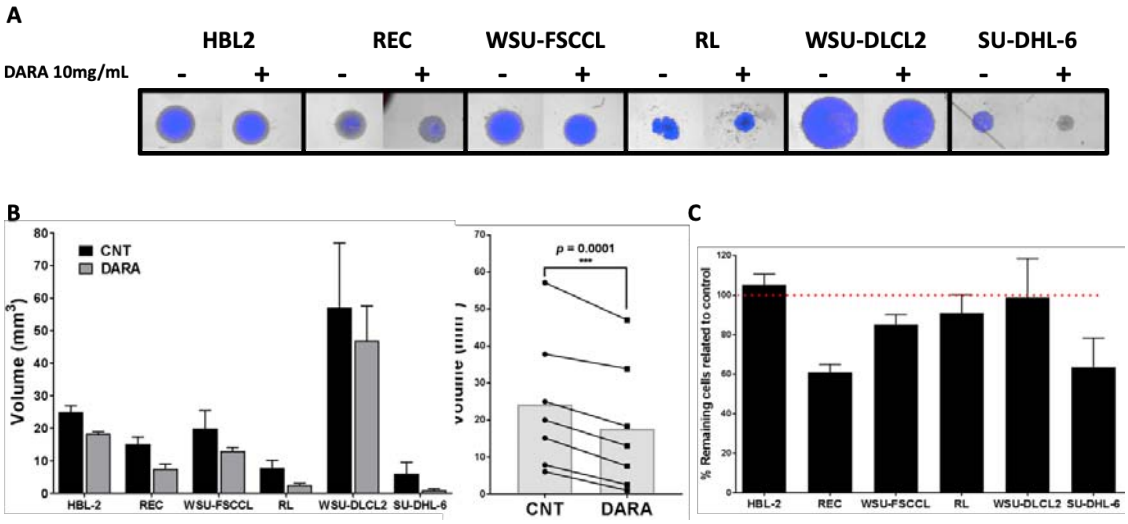

Figure S4

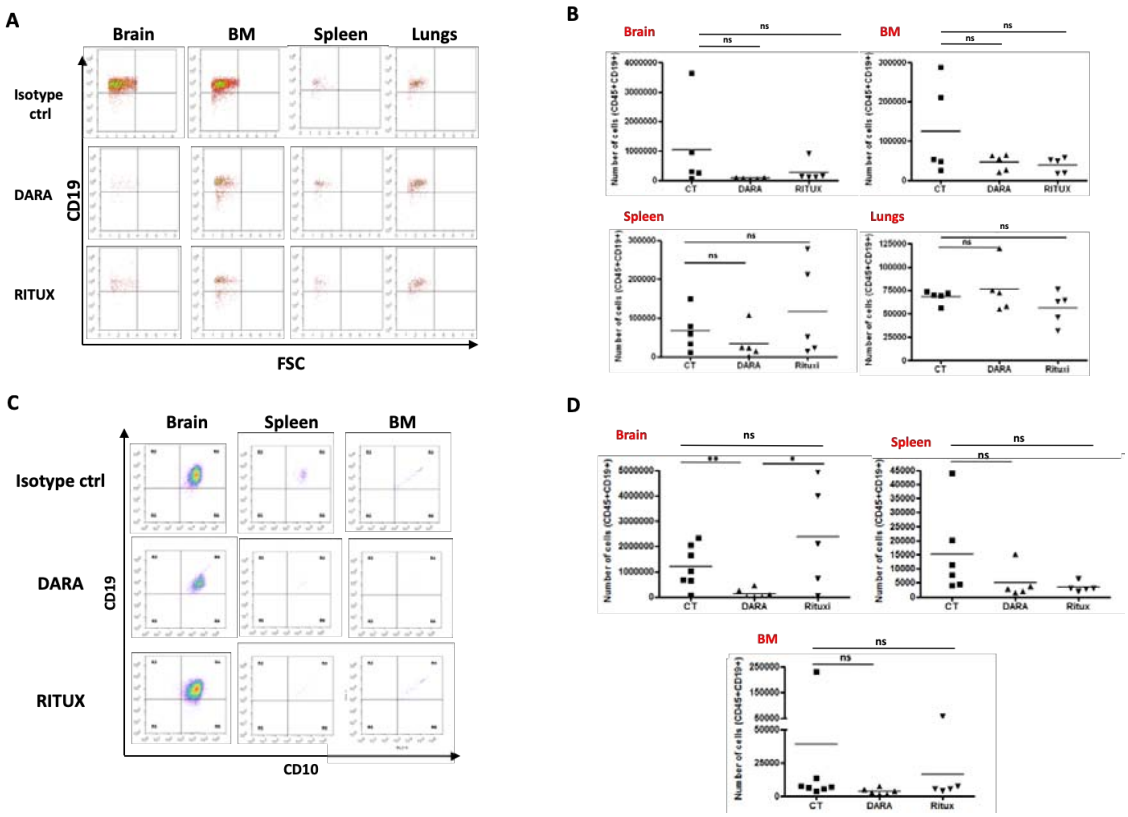

Figure S5

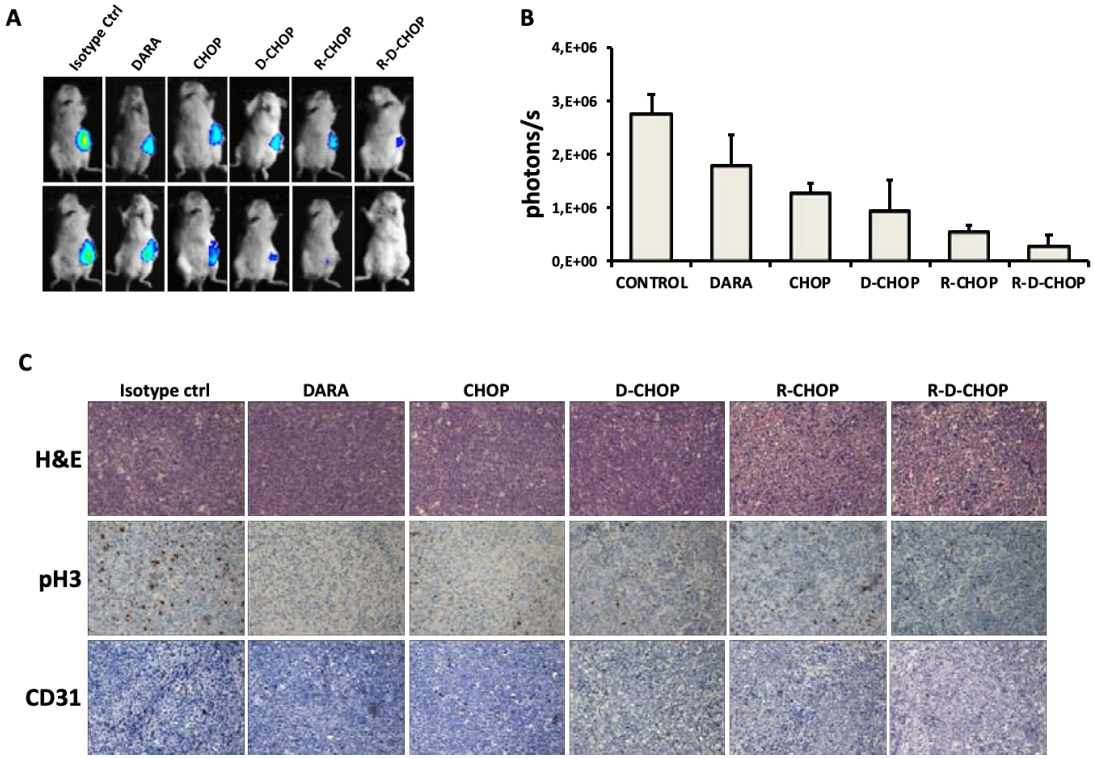

Figure S6